JGR Space Physics

RESEARCH ARTICLE
10.1029/2022JA030874

Key Points:

- Plateau-like magnetic-field spectra with triple power laws are ubiquitous in the Martian magnetosheath
- Comprehensive statistical results suggest strong correlations between the plateau occurrence rate and pickup ion related parameters
- The formation of plateau-like spectra is possibly due to energy injections from waves driven by pickup ions from Mars

Correspondence to:
H. Li,
hli@nssc.ac.cn

Citation:
Jiang, W., Li, H., Liu, X., Verscharen, D., & Wang, C. (2023). Statistical properties of plateau-like turbulence spectra in the Martian magnetosheath: MAVEN observations. *Journal of Geophysical Research: Space Physics*, *128*, e2022JA030874. https://doi.org/10.1029/2022JA030874

Received 26 JUL 2022
Accepted 23 DEC 2022

The copyright line for this article was changed on 19 JAN 2023 after original online publication.

Statistical Properties of Plateau-Like Turbulence Spectra in the Martian Magnetosheath: MAVEN Observations

Wence Jiang[1,2,3], Hui Li[1,2], Xiaodong Liu[1,2], Daniel Verscharen[3], and Chi Wang[1,2]

[1]State Key Laboratory of Space Weather, National Space Science Center, CAS, Beijing, China, [2]University of Chinese Academy of Sciences, Beijing, China, [3]Mullard Space Science Laboratory, University College London, Dorking, UK

Abstract The Martian magnetosheath provides us with a natural laboratory to study plasma turbulence in the presence of pickup ions and locally generated instabilities. Unlike the typical magnetic-field spectra with a single spectral scaling at magnetohydrodynamics (MHD) scales in Earth's magnetosheath, the magnetic-field spectra in the Martian magnetosheath during 4 years of Mars Atmosphere and Volatile EvolutioN observations frequently present an additional spectral break-point with a shallow slope at MHD scales which we define as a plateau-like spectral feature. The average occurrence rate of plateau-like magnetic-field spectra is 56.6% of our measurement intervals. At moderate pick-up angles, the occurrence rate increases to a maximum of ~70.0%. Furthermore, we present a positive correlation with the local ion density and anti-correlations with the local β_i and the solar Extreme Ultra Violet irradiance. A similar occurrence rate in the quasi-perpendicular and the quasi-parallel magnetosheath (60.1% vs. 52.9%) indicates that the plateau-like spectra are more likely formed locally than in the upstream solar wind. Our results suggest that energy injection from pickup ion driven micro-instabilities, for example, in the form of proton cyclotron waves, has insufficient time to evolve into a fully developed cascade in such a confined space like the Martian magnetosheath.

Plain Language Summary Magnetic-field turbulence is ubiquitous in planetary plasma environments. However, our current understanding of turbulence injection and dissipation in the magnetosheath is still very limited. At Mars, the far-extended neutral exospheres of hydrogen and oxygen provide an extraordinary environment to study the energy injection into the background turbulence by pickup ions. Our statistical study reveals that a large fraction of the observed magnetic-field spectra exhibit a triple power-law with a broadband plateau-like feature. We quantify the occurrence of plateau-like spectra and correlate it with pickup-ion-related parameters. We find that strong energy injection driven by pickup ions, including but not limited to proton cyclotron waves, creates these plateaus. The generated waves cannot evolve into a fully developed cascade given the insufficient spatial extent of the Martian magnetosheath.

1. Introduction

Compared to Earth, Mars has a smaller induced magnetosphere and a denser neutral exosphere extending outside the bow shock, making the Martian magnetosheath a more suitable natural laboratory to study turbulence in a system with strong variability, short evolution time, and abundant free-energy sources such as pickup ions. The neutral exospheres of Mars extend beyond tens of Mars radii (R_M), as revealed by the density profiles of neutral species over a wide range of altitudes derived from data provided by previous in situ spacecraft, including Phobos-2, Mars Express, and most recently, the Mars Atmosphere and Volatile EvolutioN (MAVEN) mission (Barabash et al., 1991; Chamberlain, 1963; Cravens et al., 2002; Dubinin et al., 2006; Rahmati et al., 2014). When neutral species encounter the solar wind plasma flow, they are ionized at a rate that depends on local parameters that determine charge exchange efficiency, such as density, speed, and temperature (Cravens et al., 1987; Fite et al., 1960). Subsequently, the newly ionized ions are accelerated by the solar wind convection electric field, producing pickup ions with a ring-beam velocity distribution function (VDF). Other ionization mechanisms, such as photo-ionization by solar extreme ultra-violet (EUV) radiation, also contribute and resulting in seasonal variations of the pickup ion densities (Modolo et al., 2005; Rahmati et al., 2014, 2017, 2018; Romanelli et al., 2016).

Because of the way the pickup ions are produced, they naturally present proton temperature anisotropy with $T_{i\perp} \neq T_{i\parallel}$, where $T_{i\perp}$ ($T_{i\parallel}$) is the proton temperature in the direction perpendicular (parallel) to the background magnetic field. The ring beam VDF of the pickup ions in velocity space is unstable to micro-instabilities, such as the ion cyclotron instability and the mirror instability (Cowee et al., 2008; Cowee & Gary, 2012; Gary, 1991;

Huddleston et al., 1999; Matteini et al., 2015; Russell et al., 1999). These instabilities generate short-wavelength fluctuations and reduce the free energy by scattering the pickup ions toward a more isotropic distribution in velocity space. The properties of pickup ions and the growth of ion anisotropy instabilities depend on the local plasma parameters, such as the pickup angle (α_{BV}, the angle between the local plasma velocity, $\mathbf{V}_i$, and the background magnetic field, $\mathbf{B}$), the local number density n_i and β_i, where $\beta_i = 2\mu_0(n_i k_B T_i)/|B|^2$, μ_0 is the vacuum permeability, k_B is the Boltzmann constant, T_i the local ion temperature, and μ_0 is the magnetic field strength (Cowee & Gary, 2012; Gary et al., 1993). The ion ring-beam instability generates significant magnetic-field fluctuations at frequencies below the proton cyclotron frequency in the form of proton cyclotron waves (PCWs), which have been frequently observed in the Martian environment (Andrés et al., 2020; Brain, 2002; Delva et al., 2015; Harada et al., 2019; Romanelli et al., 2013). If created by anisotropy instabilities, PCWs propagate predominantly in the direction parallel to the background magnetic field with a left-hand polarization (Gary & Madland, 1988; Huddleston et al., 1999). The occurrence rate of PCWs depends on the seasonal variation of the solar EUV irradiance at Mars, the dynamic pressure of the solar wind, and its Alfvén Mach number (Harada et al., 2019; Romanelli et al., 2013).

In planetary environments, magnetic-field fluctuations with a narrow-band "bump" in the power spectral density (PSD) are often attributed to the presence of locally generated waves. Apart from the narrow-band spectral "bump", scale-invariant scalings such as the Kolmogorov $f^{-5/3}$ scaling of the magnetic-field fluctuations are important characteristics of turbulence with an inertial energy cascade from large scales to small scales (Bruno & Carbone, 2013; Sahraoui et al., 2020; Tu & Marsch, 1995; Verscharen et al., 2019). The PSDs of the magnetic-field fluctuations in the magnetosheath present a f^{-1} scaling at MHD scales around Earth (Alexandrova, 2008; Czaykowska et al., 2001; Huang et al., 2017; Li, Jiang, et al., 2020), Saturn (Hadid et al., 2015), Mercury (Huang et al., 2020), Venus (Dwivedi et al., 2015; Terres & Li, 2021; Vörös et al., 2008a, 2008b) and Mars (Lentz et al., 2021; Ruhunusiri et al., 2017). The absence of a Kolmogorov scaling suggests the absence of a fully developed inertial-range cascade of energy. However, the physical mechanism for the existence of a broad-band f^{-1} scaling rather than a $f^{-5/3}$ scaling in planetary magnetosheath remains an open question.

In addition to the effects of quasi-parallel/quasi-perpendicular bow shock interactions, pickup-ion related energy injections potentially also contribute to the properties of the turbulence such as the broad-band spectral behavior and the nonlinear energy cascade rate. Ruhunusiri et al. (2017) show that the magnetic-field spectra are significantly flattened at MHD scales, which is similar to the results reported in other planetary magnetosheath. This effect is more prominent when Mars is closer to the sun, which is likely related to the presence of more PCWs as suggested by Romanelli et al. (2016). However, the physics of the interaction between coherent waves such as PCWs and background turbulence is not clear. 1D hybrid simulations show that the energy injected by pickup ion instabilities can inversely cascade to smaller wave numbers (Cowee et al., 2008; Gary & Winske, 1993), although observational evidence for this process is lacking. Romanelli et al. (2022) suggest that PCWs do not have a significant effect on the in-compressible cascade rate, casting doubts on the modification of turbulence in the presence of PCWs.

In this study, we focus on the broad-band behavior of PSDs, quantify the statistical properties of the magnetic-field spectra in the Martian magnetosheath, and investigate the impact of pickup ions on the turbulent spectra. We discuss the origin of strong energy injections near ion scales and present comparisons between results downstream and upstream of quasi-parallel and quasi-perpendicular bow shock geometries.

2. Data Set and Methodology

We use plasma data provided by the Solar Wind Ion Analyzer (SWIA) (Halekas et al., 2015) and the Suprathermal and Thermal Ion Composition (STATIC) sensor (McFadden et al., 2015), magnetic field data provided by the Magnetometer instrument (MAG) (Connerney et al., 2015), and EUV irradiance data at the wavelength of 121–122 nm provided by the Extreme Ultra-Violet Monitor (EUVM) (Eparvier et al., 2015) onboard MAVEN (Jakosky et al., 2015) from January 2015 to November 2019. Bow shock crossings are characterized by sudden and sharp increases in plasma density and temperature with significant decreases in plasma bulk velocity. The magnetic, dynamic, and thermal pressures are balanced at the magnetic pile-up boundary (MPB). Therefore, we identify MPB crossings when the threshold condition $\beta^* = 2\mu_0(n_i k_B T_i + P_d)/|B|^2 = 1$ is satisfied, where $P_d = n_i V_i^2/2$ is the dynamic pressure and V_i is the local plasma bulk velocity. Matsunaga et al. (2017) find that the pressure balance boundary defined by $\beta^* = 1$ tends to be located at higher altitudes than the induced

magnetosphere boundary and the ion composition boundary. Thus, we use $\beta^* = 1$ to identify the MPB to reduce the interference of Martian ionospheric activities throughout this study.

We perform a fast Fourier transform for each magnetosheath segment using Welch's method to obtain the omni-directional PSD of the magnetic-field fluctuations (Li, Jiang, et al., 2020). The magnetic field data have a temporal cadence of 1/32 s, yielding a Nyquist frequency of 16 Hz, sufficient for studying the physical processes at sub-ion scales in this environment. Generally, the PSD of magnetic field fluctuations in the solar wind exhibit only one break-point (f_{bk}) at frequencies around $f_{\rho i}$ and f_{di}. Under Taylor's frozen-in hypothesis (G. I. Taylor, 1937), these frequencies are defined by the corresponding scales as $f_{\rho i} = V_i/2\pi\rho_i$ and $f_{di} = V_i/2\pi d_i$, where $\rho_i = V_{th\perp}/\Omega_i$ is the proton gyro-radius, Ω_i is the proton gyro-frequency, $V_{th\perp}$ is the thermal speed of the protons, $d_i = V_A/\Omega_i$ is the proton inertial length and V_A is the Alfvén speed.

3. Plateau-Like Spectra in the Martian Magnetosheath

Instead of the usual turbulence spectra with a single break-point at ion-kinetic scales, we find that PSDs in the Martian magnetosheath additionally break-point at a frequency well below the typical break-point frequency near ion scales. This behavior leads to plateau-like spectra consisting of three distinct spectral ranges with three distinct spectral indices. Thus, the double power-law fitting technique fails to evaluate the power-law behaviors and spectral characteristics. We implement an automatic procedure to determine the two break-point frequencies, f_{bk1}, f_{bk2}, and obtain the three spectral indices, α_1, α_2, and α_3, by minimizing the sum of the chi-square values in a triple power-law fitting technique. The whole frequency range in our fitting procedure ranges from 0.001 to 5.0 Hz, which covers the Martian system scale and sub-ion scales assuming the Taylor hypothesis. To guarantee reliable power-law fitting at ultra-low frequencies (e.g., <0.01 Hz), only segments with a duration greater than 20 min are used. We choose a confidence interval of the fitting greater than 99.9%.

3.1. Overview of a Plateau-Like Spectrum Case

Figure 1 shows a typical magnetosheath crossing event observed by MAVEN on 4 June 2016. Figures 1a–1d give the magnetic field in MSO coordinates, the ion number density, and ion bulk velocity in MSO coordinates, and β^*, respectively. The magnetosheath interval is marked by two vertical dashed lines in red. MAVEN enters the magnetosheath from the upstream solar wind at around 21:10:00 UT with sudden enhancements in the magnetic field, ion density, and velocity perturbations. The ion differential energy spectrogram measured by SWIA indicates significant heating of ions after the bow shock crossing. At 22:43:00 UT, MAVEN crosses the MPB where $\beta^* = 1$ with a sudden decrease in ion velocity. As shown in Figure 1e, there are many ions in the field-of-view of SWIA with an energy greater than that of the thermal protons of the solar wind in the sheath region, but less than the calculated maximum energy of the locally generated pickup O^+ (H^+) as denoted by the red (black) line. This finding suggests the existence of varying pickup ions with a mass greater than hydrogen.

The maximum energy of the pickup O^+ (red) and H^+ (black) is calculated by $E_{max} = 2mV_i^2\sin^2\alpha_{BV}$, where m is the mass of the specific ion and α_{BV} is the angle between the magnetic field and the solar wind velocity. From the ion mass spectrogram retrieved from STATIC shown in Figures 1f and 1a significant enhancement of pickup atomic oxygen (16 amu) can be easily identified, especially at around 22:30:00 UT. Furthermore, according to Rahmati et al. (2017), these pickup atomic oxygen ions are most likely O^+. However, pickup H^+ is hardly discriminated against the thermal protons of the solar wind. Therefore, we show the VDF of the ions in the plane ($v_\parallel$, $v_{\perp V}$) retrieved from SWIA in Figure 1k from 22:28:03 UT to 22:28:07 UT, where $v_\parallel$ is the velocity of the ions parallel to the magnetic field and $v_{\perp V}$ is the velocity of ions parallel to the direction of $\hat{b} \times (\hat{b} \times V)$, where $\hat{b}$ is the unit vector of the magnetic field. The dotted circles indicate the maximum energy of pickup O^+ (green) and H^+ (red) in the spacecraft frame. In Figure 1k, there are clear signatures of the pickup H^+ population near the red circle and of the pickup O^+ population near the green circle. These pickup ions are highly unstable and capable of exciting various types of kinetic waves that inject energy into the magnetic-field spectra at specific frequencies. The local average parameters during this magnetosheath interval are $n_i = 2.43\ cm^{-3}$, $V_i = 230.3$ km/s, $B = 5.8$ nT, $T_p = 49.9$ eV (proton temperature), $T_e = 14.4$ eV (electron temperature), $M_A = 2.9$ (Alfvén Mach number), and $\beta_i = 1.8$. The gyro-radius of the ion ρ_i and the inertial length of the ion d_i are 216.4 and 189.5 km, respectively.

As shown in Figure 1j, two break-point frequencies at $f_{bk1} = 0.009$ Hz and $f_{bk2} = 0.12$ Hz divide the PSD into three parts with different spectral indices, $\alpha_1 = -1.8$, $\alpha_2 = -0.3$, and $\alpha_3 = -3.0$. We refer to this kind of spectrum

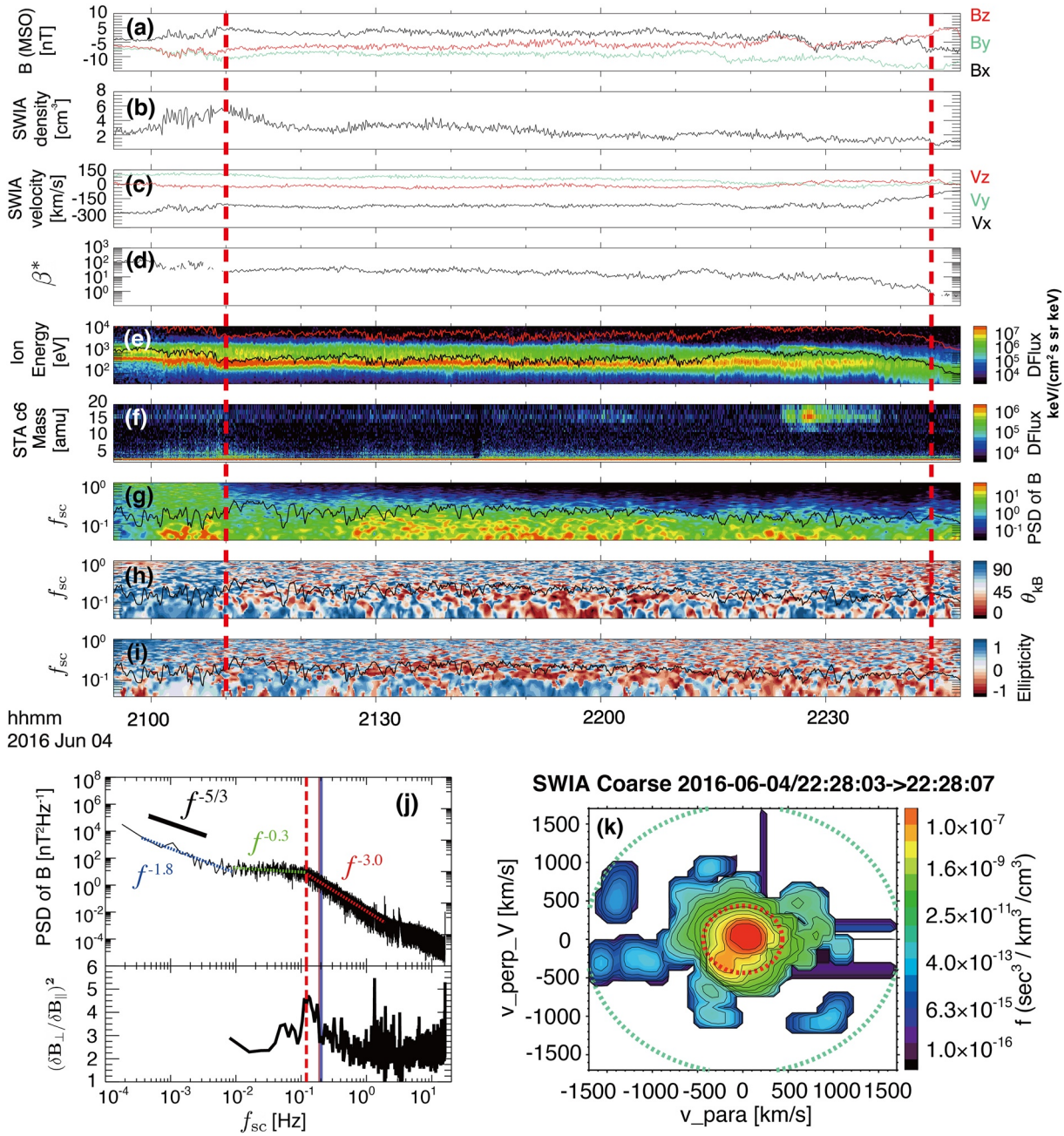

Figure 1. Mars Atmosphere and Volatile EvolutioN observations of the Martian magnetosheath crossing event on 4 June 2016. The magnetosheath interval is denoted by two vertical dashed lines in red. (a) Magnetic field in MSO coordinates from MAG. (b) Number density of ions from Solar Wind Ion Analyzer (SWIA). (c) Bulk velocity of ions in MSO coordinates from SWIA. (d) β^*. (e) Differential energy flux spectrogram of ions from SWIA. The maximum energy of pickup O^+ and H^+ are denoted by the lines in red and black. (f) Mass spectrogram of ions from STATIC. (g) Power spectral density spectrogram of the magnetic field. (h) Wave normal angle θ_{kB}. (i) Ellipticity. The black lines in (g, h, and i) represent the Doppler-shifted proton cyclotron frequency. (j) PSD of the magnetic field within the magnetosheath interval. Vertical lines denote the characteristic ion-scale frequencies $f_{\rho i}$ (light red), f_{di} (light blue), and f_{bk2} (red dashed line). (k) Velocity distribution function of the ions in the plane of $(v_{\parallel}, v_{\perp V})$ retrieved from SWIA data from 22:28:03 to 22:28:07. The dotted circles represent the maximum pickup energy of H^+ (red) and O^+ (green).

as a ''plateau-like spectrum" in this study. $f_{\rho i}$ and f_{di} are both ~0.2 Hz and are indicated by solid vertical lines in brown and blue in Figure 1j. Around f_{bk2} (0.12 Hz, indicated by the red dashed line), the ratio of transverse to compressive fluctuation power $\left((\delta B_{\perp}/\delta B_{\parallel})^2\right)$ increases to ~5.

To understand the nature of the plateau-like magnetic-field spectrum, we apply the singular value decomposition method to obtain the wave properties, such as the wave power, wave normal angle, and ellipticity shown in

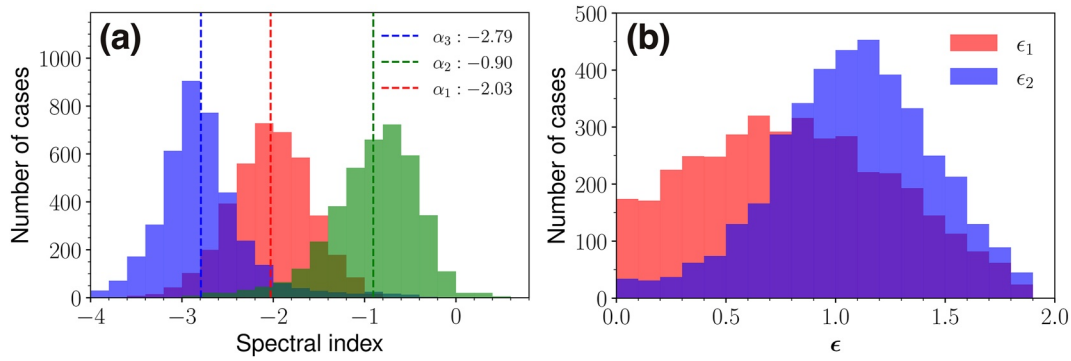

Figure 2. Histogram of the magnetic-field spectral indices α_1, α_2, and α_3 (a) and the normalized differences ϵ_1 and ϵ_2 (b). The dashed lines indicate the mean values of the spectral indices.

Figures 1g–1i. The Doppler-shifted local proton cyclotron frequency (f_{ci}), indicated by the black line, is calculated with the method used by Jian et al. (2010). Below f_{ci} and around f_{bk2}, we identify wave activity (PSD greater than 10 nT^2/Hz) with left-hand polarization (ellipticity close to −1) and quasi-parallel propagating (θ_{kB} close to 0). These fluctuation features are consistent with the properties of PCWs. In this case, the MAVEN spacecraft is located in the magnetosheath downstream of a quasi-perpendicular bow shock, which provides a favorable environment for the excitation of PCWs (Harada et al., 2019). PCWs possibly generate the plateau-like magnetic-field spectrum, since their power typically increases around this frequency range. The $f^{-1.8}$ scaling for ultra-low frequencies (<0.01 Hz) possibly originates from the solar wind, suggesting that the large-scale solar wind turbulence is conserved during the bow shock crossing in this frequency range. The spectral scaling at kinetic scales follows $f^{-3.0}$, consistent with energy dissipation at kinetic scales. These are similar to our previous results obtained in the Earth magnetosheath, especially close to the bow shock (Li, Jiang, et al., 2020).

3.2. Occurrence Rate of Plateau-Like Spectra

We calculate two break-point frequencies and three power spectral indices for each PSD of 3955 magnetosheath segments. Figure 2a shows the histograms of the magnetic-field spectral indices. The mean values and standard deviations are $\alpha_1 = -2.03 \pm 0.44$, $\alpha_2 = -0.90 \pm 0.5$, and $\alpha_3 = -2.79 \pm 0.53$. The averaged break-point frequencies are $f_{bk1} = 0.007$ Hz and $f_{bk2} = 0.574$ Hz. Statistically, the normalized $f_{bk2}/f_{\rho i}$ is close to unity, indicating that the magnetic-field spectra break-point near the proton gyro-scale. To exclude spectra that do not exhibit a plateau, it is essential to calculate the normalized difference ϵ_1 between α_1 and α_2, as well as the normalized difference ϵ_2 between α_2 and α_3 as.

$$\epsilon_1 = \frac{2(\alpha_2 - \alpha_1)}{|\alpha_1| + |\alpha_2|} \text{ and } \epsilon_2 = \frac{2(\alpha_2 - \alpha_3)}{|\alpha_2| + |\alpha_3|}. \quad (1)$$

By substituting the mean values of the spectral indices into Equation 1, we can derive $\epsilon_1 = 0.77$ and $\epsilon_2 = 1.02$, which we consider representative of a typical plateau-like shape. For simplicity, we use a threshold value of 0.7 to characterize plateau-like spectra. As expected, there is a negative correlation between the percentage of plateau-like events and the choice of threshold value. The percentage of plateau-like events decreases from 71.4% to 41.6% when the threshold increases from 0.5 to 0.9.

As shown in Figure 2b, the histograms of ϵ_1 and ϵ_2 peak at 0.6 and 1.1. Using a threshold of 0.7, about 56.6% of 3955 magnetosheath segments present a plateau-like shape. 28.4% of segments present only one clear spectral break-point near sub-ion scales (i.e., $\epsilon_1 < 0.7$ and $\epsilon_2 > 0.7$). Our statistics show that plateau-like spectra are prevalent in the Martian magnetosheath. This result confirms that the Kolmogorov scaling is absent in the Martian magnetosheath, which is partially in agreement with previous studies in the planetary magnetosheath (Hadid et al., 2015; Huang et al., 2017; Ruhunusiri et al., 2017). However, the plateau-like feature with an additional spectral break-point at low frequencies, suggests different origins of the magnetic-field fluctuations. The first spectral break-point represents a spatial scale comparable to the system scale of the Martian magnetosheath. The spectral scaling below the first break-point frequency reflects the processed upstream solar wind turbulence, while the plateau-like scaling is likely due to the locally developing fluctuations in the magnetosheath.

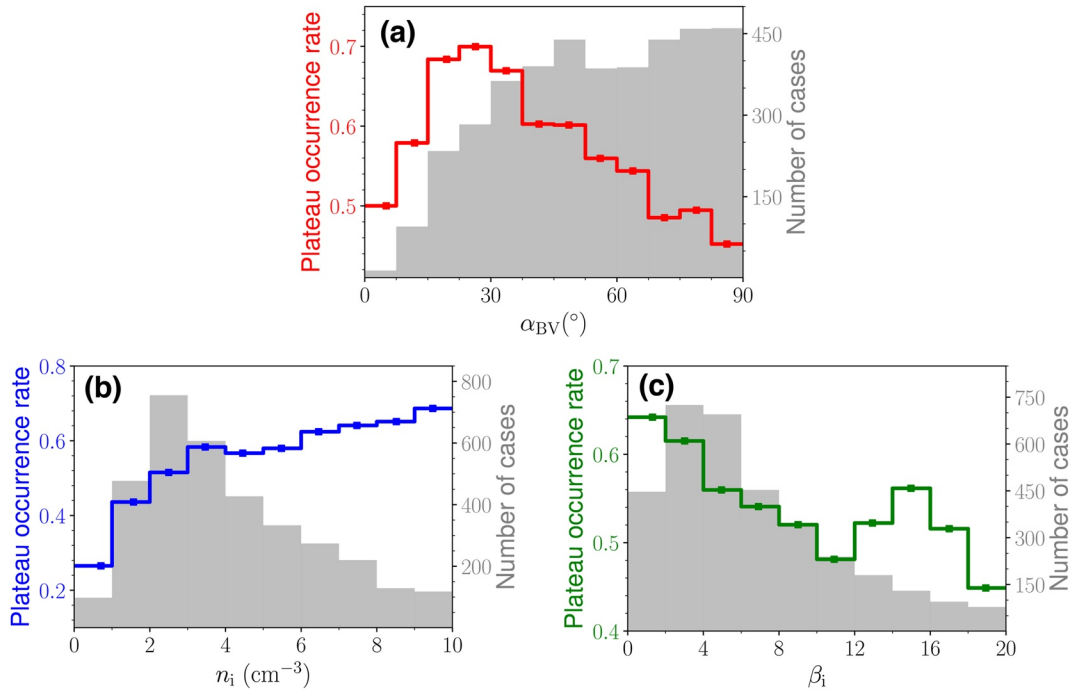

Figure 3. Statistical relations between the occurrence rate of plateau-like spectra and the pickup angle (α_{BV}), the local plasma number density (n_i) and β_i. The gray boxes denote the number of cases in each histogram bin, and the colored lines represent the occurrence rate of plateau-like spectra in the bins.

3.3. Dependence on Local Parameters

Figure 3 gives statistical relations between the occurrence rate of plateau-like spectra and the pickup angle (α_{BV}), the local plasma number density n_i and β_i. All magnetosheath segments are binned in these parameters, with the average occurrence rate of plateau-like spectra calculated accordingly.

The occurrence rate of plateau-like spectra varies as a function of α_{BV}, n_{sw} and β_i. It first increases from 50.0% to its maximum value of 70.0% as α_{BV} increases from 0° to 26°, and then decreases to 45.2% as α_{BV} increases to 90°. It also increases from 26.5% to 68.6% as n_i increases. This is possibly due to the increased pickup-ion production by charge-exchange when collisions are more frequent as the ion density increases. The occurrence rate of plateau-like spectra decreases from 64.2% to 44.9% as β_i increases to ~20, except for a minor enhancement with β_i ranging from 12 to 18. These results suggest that the plateau-like spectra are related to the properties of the pickup ions and the local β_i. The structures of the non-gyrotropic ring-beam VDF determined by α_{BV} result in different accessibility to ion micro-instabilities (Gary, 1991; Matteini et al., 2015). The occurrence rate of plateau-like spectra reaches its maximum when α_{BV} is about 26°, which is qualitatively in agreement with the highest level of saturation of PCW energy from simulations (Cowee & Gary, 2012). This result suggests that PCWs are a likely way to inject energy into such an environment.

We note that the exact determination of pickup ion species and their densities from observations in the magnetosheath is particularly difficult since a significant portion of locally generated pickup H^+ is buried in thermal protons. Therefore, we use n_i and α_{BV} as proxyes for the properties of the pickup ions.

3.4. Dependence on Solar EUV Irradiance

The density of pickup ions and relative percentages of different ion species exhibits seasonal variations, which is due to the EUV irradiance at Mars varying with distance to the Sun (Rahmati et al., 2017). From January 2015 to November 2019, Mars has revolved around the Sun for nearly 2.7 cycles, making it possible to investigate the dependence of the occurrence rate of plateau-like spectra on the EUV irradiance at Mars.

As shown in Figure 4a, the EUV irradiance at Mars varies with Mars' solar longitude (L_s), representing a significant seasonal variation with a maximum value near perihelion ($L_s \approx 255°$) and a minimum value near aphelion

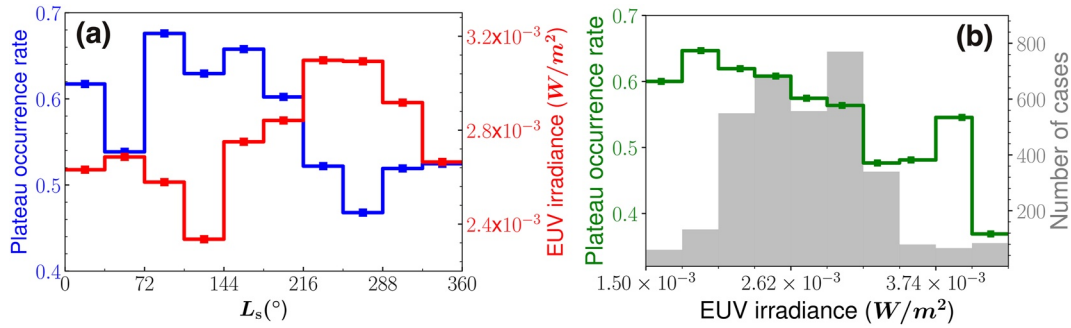

Figure 4. (a) The occurrence rate of the plateau-like spectra and Extreme Ultra Violet (EUV) irradiance in H I Lyman-α as a function of solar longitude (L_s). (b) The occurrence rate of the plateau-like spectra as a function of the EUV irradiance and histogram of the EUV irradiance.

($L_s \approx 90°$). The occurrence rate of the plateau-like spectra also presents a significant seasonal variation but is out of phase with the EUV irradiance. The occurrence rate near the aphelion is 64.7% and decreases to 47.6% near the perihelion. Figure 4b shows that the occurrence rate of plateau-like spectra decreases with increasing EUV irradiance, from 64.7% to 45.7% when the EUV irradiance increases from 1.92×10^{-3} W/m^2 to 4.3×10^{-3} W/m^2. Although the uncertainty of the occurrence rate for each bin increases when the corresponding case number decreases, the negative correlation between the occurrence rate of plateau-like spectra and the EUV irradiance is clear.

This inverse correlation between the plateau occurrence rate and the EUV irradiance suggests that pickup-ion-related waves modulate the formation of plateau-like spectra. According to the exosphere model (Chaufray et al., 2015), as Mars moves closer to the sun, the density of escaped atomic hydrogen increases by a factor of 8 during the winter solstice. Thus, more pickup H^+ and related waves can be formed in the magnetosheath, which potentially evolves in space and time under different upstream and EUV conditions.

3.5. Dependence on Upstream Conditions

To characterize different conditions of the upstream solar wind, we first remove contamination from fore-shock perturbations. We apply an automatic algorithm to determine the pristine solar wind based on the solar wind bulk speed (V_{sw}), temperature (T_{sw}), normalized root-mean-squared magnetic fluctuation level (σ_B/B_{sw}), and spacecraft latitude (L). The pristine solar wind satisfies $V_{sw} > 200$ km/s, $V_{th}/V_{sw} < 0.1$, $\sigma_B/B_{sw} < 0.15$, and $L > 500$ km (here V_{th} is the thermal speed of the protons, σ_B is the root-mean-squared value of the magnetic field fluctuations), which reliably rule out contamination from the fore-shock and the magnetosheath, see Halekas et al. (2017) for more details. We use the Mars Solar Electric (MSE) coordinate system here, in which the X axis points toward the Sun, and the Y axis is aligned with the perpendicular component of the upstream magnetic field (B_{sw}) to the X axis. The Z axis is aligned with the upstream convective electric field ($\mathbf{E}_{sw} = -\mathbf{V}_{sw} \times \mathbf{B}_{sw}$). With only single-spacecraft data available, we use same-orbit measurements to determine the upstream parameters assuming a steady solar wind condition.

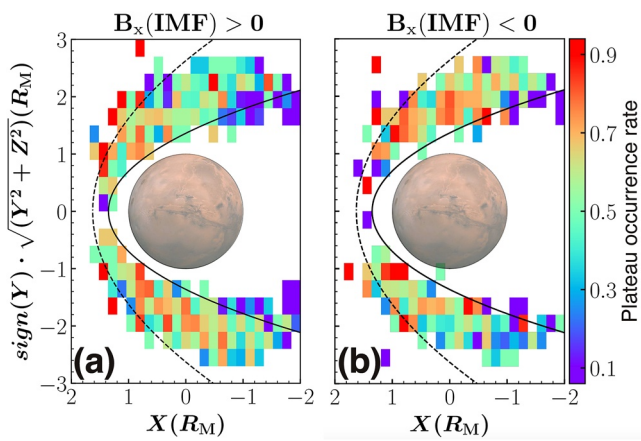

Figure 5. Statistical maps of the plateau occurrence rate in the Mars Solar Electric coordinate system. (a) 2D distribution of the occurrence rate for B_x(IMF) > 0 and (b) for B_x(IMF) < 0.

Figures 5a and 5b shows spatial distributions of the occurrence rate of plateau-like magnetic-field spectra in the MSE coordinate system. We separate different shock geometries by dividing the data set into two sub-sets using the sign of the X component of the upstream magnetic field (B_x(IMF)). The hemisphere with $Y < 0$ denotes the quasi-perpendicular magnetosheath when B_x(IMF) > 0 and the quasi-parallel magnetosheath when B_x(IMF) < 0. The situation is the opposite in the hemisphere with $Y > 0$. We bin the data sets in the $X - R$ plane of the MSE coordinate system and calculate the occurrence rate of plateau-like spectra in each bin. Bins with only one case are not shown. As seen in the distribution map, plateau-like spectra more frequently

occur in the magnetosheath downstream of a quasi-perpendicular bow shock, especially in the center of the flank, suggesting that the quasi-perpendicular bow shock favors the occurrence of plateau-like spectra. However, the difference is not particularly strong considering the average occurrence rate, which is 60.1% in the magnetosheath downstream of a quasi-perpendicular bow shock and 52.9% in the magnetosheath downstream of a quasi-parallel bow shock. This trend differs from the previous investigation on the MHD-scale spectral slope in the Martian magnetosheath (Ruhunusiri et al., 2017). They use a single spectral slope to fit the PSDs at MHD scales, while we implement double spectral slopes after inspecting the general behavior of the magnetic-field PSDs in the magnetosheath. Furthermore, our study takes into account much lower frequencies than in the previous work.

These findings suggest that the quasi-perpendicular bow shock favors the occurrence of plateau-like spectra. Plateau-like spectra are more likely to form locally than from the upstream solar wind since more PCWs are generated in the foreshock region. There is no obvious asymmetry between the $Z < 0$ and $Z > 0$ hemispheres, suggesting that the direction of the upstream convection electric field has no significant impact on the occurrence of plateau-like spectra. However, in the far flank of the magnetosheath, the occurrence rate of plateau-like spectra is systematically reduced. This result also supports previous analyses on the evolution of the Earth's magnetosheath (Huang et al., 2017; Li, Jiang, et al., 2020), where the Kolmogorov scaling can be recovered after sufficient time for the turbulence to develop.

4. Discussion and Conclusions

Mars has a small induced magnetosphere and a neutral exosphere extending outside the bow shock. Thus, high-abundance pickup ions around Mars are an important type of free energy source for energy injection. Focusing on the magnetosheath, we show that the magnetic-field spectra frequently exhibit triple power laws with an additional spectral break-point at MHD scales. This triple power law behavior is marked by significantly shallower spectral scaling at MHD scales (defined as a plateau-like spectrum), which has an overall occurrence rate of 56.6%. Our observations of plateau-like spectra over a large frequency range ($10^{-3} - 10^{1}$ Hz) confirm previously reported observations of similar spectral features at MHD scales, for example, ion-flux fluctuations in the Earth's magnetosheath (Rakhmanova et al., 2018, 2020; Riazantseva et al., 2016), magnetic-field fluctuations in the Venusian and Martian magnetosheath (Lentz et al., 2021; Terres & Li, 2021). Our study focuses on the broadband plateau-like spectral characteristic and suggests that the formation of plateau-like spectra could be due to various energy injections by pickup ions from Mars. As shown in our case study, energy injection in the form of PCWs generated by pickup ions and possible inverse energy transfer to low frequencies may be responsible for the formation of plateau-like spectra. We further support this interpretation with statistical evidence based on MAVEN data.

Plateau-like spectra are most frequently observed when the local pickup angle (α_{BV}) is moderate at about 26°. In this case, the occurrence rate is 70.0%, greater than the overall occurrence rate of 56.6%. The increase of α_{BV} represents that the ion ring-beam distribution changes from a beam-like distribution with a large parallel component to a ring-like distribution with a large perpendicular velocity in velocity space. In simulations depending on α_{BV}, the total energy density of the fluctuating magnetic-field saturates at a higher level when $\alpha_{BV} \sim 30°$ (Cowee & Gary, 2012). As α_{BV} increases, the frequency of waves generated by the ring-beam instability with the largest growth rate transits to lower frequencies (Gary & Madland, 1988; Huddleston et al., 1997; Matteini et al., 2015). When the frequency of maximum energy injection moves to lower frequencies, the shape of the magnetic-field spectrum becomes less plateau-like.

The occurrence rate of plateau-like spectra in the magnetosheath increases with n_i. This result indicates that plateau-like spectra are generated by waves driven by pickup ions, since more neutral particles can be ionized through the charge exchange process when n_i increases. However, it is difficult to determine the exact percentage of pickup ions. The pickup H^+ populations are usually hidden by the background thermal protons since their energy ranges overlap. The method used by Rahmati et al. (2017) inspecting different anodes away from the bulk flow direction cannot accurately extract pickup populations from the thermal protons. Furthermore, we find that the occurrence rate of plateau-like spectra decreases with the local β_i in the magnetosheath, which is consistent with the theoretical prediction as well as observational evidences for the ion cyclotron instability damping and a transition to mirror-mode instability in high β_i plasma (Anderson & Fuselier, 1993; Gary et al., 1993).

However, PCWs are not the only possible contributors to the formation of a plateau-like spectrum since we also observe some plateau-like spectra without obvious PCW features. For some events with $\beta_i \sim 15$, we identify

fast and slow waves at the typical plateau frequencies. These wave modes potentially contribute to the peak of the plateau occurrence rate near $\beta_i \sim 15$ shown in Figure 3c. We illustrate this issue in Figure 6, which shows an event of a plateau-like magnetic-field spectrum with $\beta_i \sim 16$. The magnetic-field fluctuations are enhanced significantly at frequencies in the plateau range (i.e., $3 \times 10^{-2} - 3 \times 10^{-1}$ Hz), which is indicated by enhanced power in Figure 6g. From Figures 6d and 6e, no obvious PCWs are found for this case. Combining measurements of ion moments and the magnetic field, we apply the method proposed by Li, Li, et al. (2020) to diagnose the wave modes of the analyzed fluctuations. We find the existence of fast-mode and slow-mode waves in the band-pass signals with periods of 8–16 s in Figure 6h. The fluctuations in density and the magnetic field strength are positively correlated (CC = 0.7) in the blue-shaded region, while they are anti-correlated (CC = −0.6) in the red-shaded region. At the same time, the perpendicular (parallel) velocity fluctuations are correlated with the density fluctuations with CC = 0.6 (CC = −0.7), indicating the existence of fast (slow) waves.

The occurrence rate of the plateau-like spectra is anti-correlated with the EUV irradiance at Mars. Since Solar EUV irradiance increases as the Mars-Sun distance decreases, more heavy species such as oxygen are photo-ionized and become pickup ions in the magnetosheath (Modolo et al., 2005; Rahmati et al., 2017). With the inclusion of heavy pickup ions, such as pickup O^+, the ion cyclotron instability can be significantly suppressed (Cowee et al., 2008; Gary et al., 1993; Remya et al., 2013). Harada et al. (2019) find that the occurrence of PCWs in the Martian magnetosheath decreases with solar EUV irradiance. The density of pickup ions and their relative density ratio are sensitive to the variation of EUV irradiance. Our finding further supports that the pickup-ion instabilities and the related wave evolution are linked to the occurrence of plateau-like spectra.

The average occurrence rate of plateau-like spectra is 60.1% and 52.9% in the magnetosheath downstream of the quasi-perpendicular and quasi-parallel bow-shock geometries. Although the difference is not large, the plateau-like spectra seem to occur more frequently in the magnetosheath downstream of the quasi-perpendicular shock according to the distribution map, especially in the center of the flank. This is possibly related to the finding that the ion temperature anisotropy is more significant in the magnetosheath downstream of quasi-perpendicular bow shocks, which favors the excitation of PCWs (Harada et al., 2019).

Furthermore, the plateau-like spectra preferentially link to some local generation mechanisms rather than convection from the solar wind. The occurrence rate of plateau-like spectra has no obvious preference for the magnetic-field geometry at the bow shock although that PCWs are more likely to be generated in the quasi-parallel foreshock region. Complex processes near the bow shock or the magnetopause, for example, magnetic reconnection and coherent structures, can also produce strong ion temperature anisotropy. Therefore, other forms of kinetic waves driven by ion temperature anisotropy can also contribute to the energy injection at ion scales (Anderson et al., 1994; Gary, 1991; Gary et al., 1993; Lentz et al., 2021; Maruca et al., 2018; Song et al., 1992).

Figure 7 shows location dependence of the normalized spectral break frequencies, $f_{bk1}/f_{\rho i}$ and $f_{bk2}/f_{\rho i}$, as well as their dependence on the local β_i. $f_{bk1}/f_{\rho i}$ and $f_{bk2}/f_{\rho i}$ depend significantly on the location in the magnetosheath. $f_{bk1}/f_{\rho i}$ decreases from ∼0.08 Hz in the sub-solar region to ∼0.01 Hz in the flank. $f_{bk2}/f_{\rho i}$ decreases from ∼6 Hz near the bow shock to ∼0.20 Hz in the flank. Moreover, they are both positively dependent on the local β_i. These results suggest that these two break-point frequencies evolve with the plasma convection through the Martian magnetosheath. As we discuss above, the local β_i is likely to play an essential role in modulating the wave modes which dominate locally. In this interpretation, the power injected at different frequencies causes the shifting of the plateau.

The Taylor hypothesis is mainly violated in the slow flow regime when the M_A is significantly small (Klein et al., 2014). To test the validity of the Taylor hypothesis, we calculate M_A for the data set with plateau-like spectra and for the total data set. The probability distribution of M_A is given in Figure 6a. The average M_A is about 4.5%, and 93.8% of cases have a M_A greater than 2, suggesting that the Taylor hypothesis is well satisfied here.

Figure 8b shows probability histograms of correlation coefficients between band-pass magnetic-field fluctuations, ion-velocity fluctuations $R_{\delta v_i - \delta B}$ (solid) and ion-density fluctuations $R_{\delta n_i - \delta B}$ (dotted). The frequency band is 0.001–0.015 Hz, mainly corresponding to frequencies below the first spectral break-point at MHD scales. The magnetic-field fluctuations of all magnetosheath events are moderately correlated with the ion-velocity fluctuations $\left(R_{\delta v_i - \delta B} \approx \pm 0.5\right)$, while no obvious trend is found for ion-density fluctuations $\left(R_{\delta n_i - \delta B}\right)$. These results suggest that the nature of the low-frequency magnetic-field fluctuations is likely Alfvénic, preserving the large-scale solar wind turbulence from the bow shock upstream. Due to the limitation of the cadence of particle instruments, a similar analysis is not available at kinetic scales.

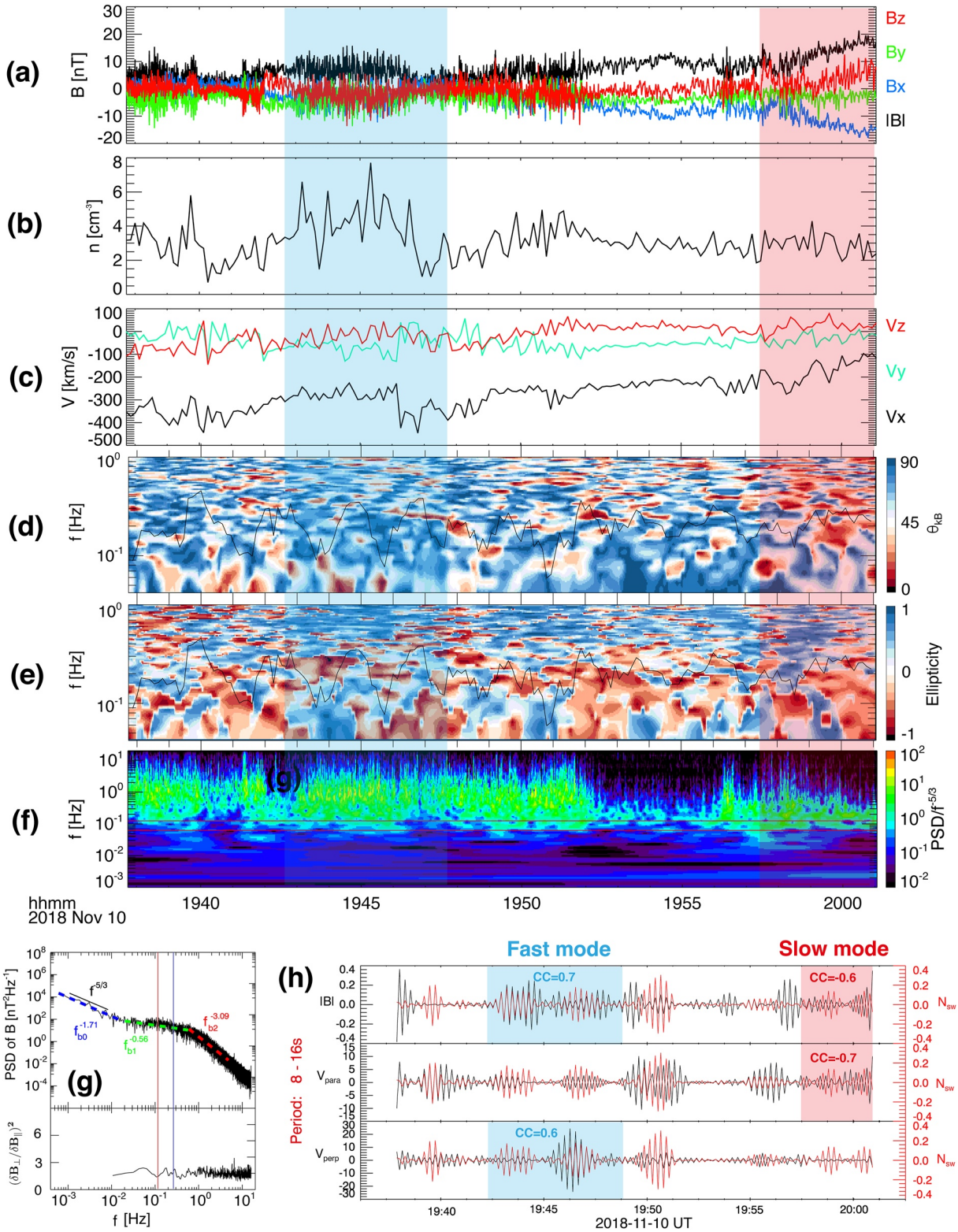

Figure 6. Mars Atmosphere and Volatile EvolutioN observations of a high β_i event on 2018 November 10. (a) Magnetic field. (b) Number density of ions. (c) Bulk velocity of ions. (d) Wave normal angle. (e) Ellipticity. (f) Wavelet power spectral density (PSD) of the magnetic-field fluctuations compensated with a Kolmogorov-like power law. Red lines denote the frequency range corresponding to time periods of 8–16 s. (g) Plateau-like magnetic-field PSD. (h) Band-pass fluctuations with periods of 8–16 s in the magnetic-field magnitude |B|, ion bulk velocity parallel (perpendicular) to the background magnetic field V_{para} (V_{perp}) and ion number density N_{sw}. Shaded areas represent segments where fast-mode waves (blue) and slow-mode waves (red) are identified.

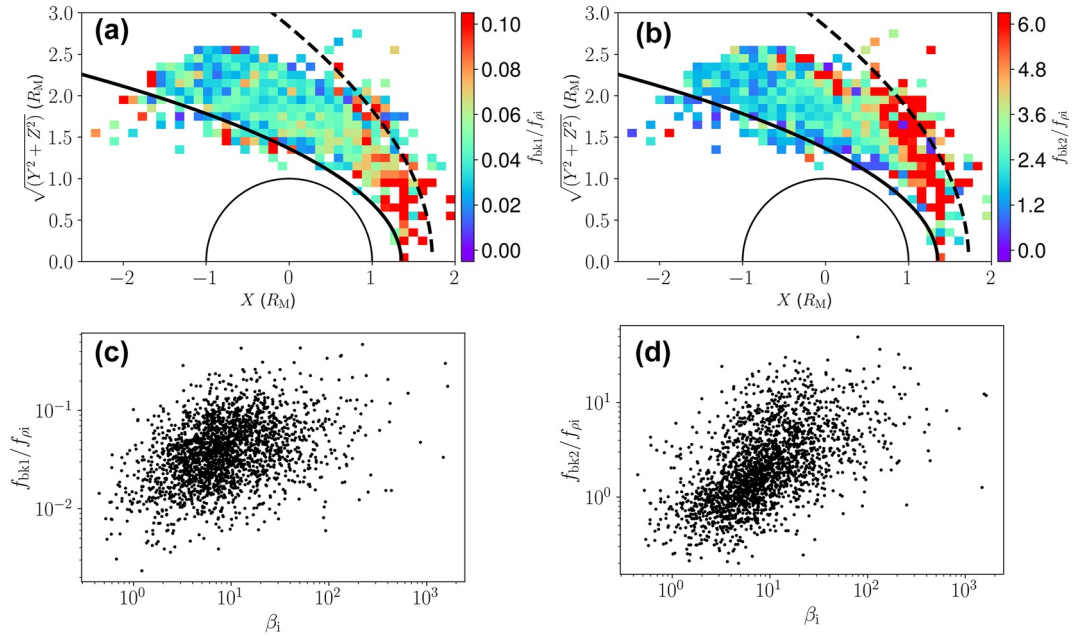

Figure 7. Break-point shifts of the plateau-like spectra. (a–b) Statistical maps of the normalized break-point frequencies $f_{bk1}/f_{\rho i}$ and $f_{bk2}/f_{\rho i}$. (c) $f_{bk1}/f_{\rho i}$ as a function of local β_i. (d) $f_{bk2}/f_{\rho i}$ as a function of local β_i.

To conclude, our results suggest that the deviation of the Martian magnetosheath turbulence from the Kolmogorov $f^{-5/3}$ scaling is due to energy injection brought by ion/pickup ion micro-instabilities. In this scenario, pickup-ion related waves (e.g., PCWs) are responsible for the formation of the plateau-like spectra. Future detailed studies involving wave-mode/structure identifications are needed for a better understanding of the detailed nature of the plateau. Our results furthermore suggest that the spatially small and confined Martian magnetosheath does not provide sufficient space for locally injected waves to evolve and join the background inertial-range cascade with a Kolmogorov $f^{-5/3}$ scaling. However, the question as to how the newly injected energy evolves, for example, via a cascade or an inverse cascade (Pouquet et al., 1976, 2020), remains unknown. Further detailed investigations into the evolution of plateau-like magnetic-field spectra and energy transfer mechanisms of waves in a turbulent background are needed.

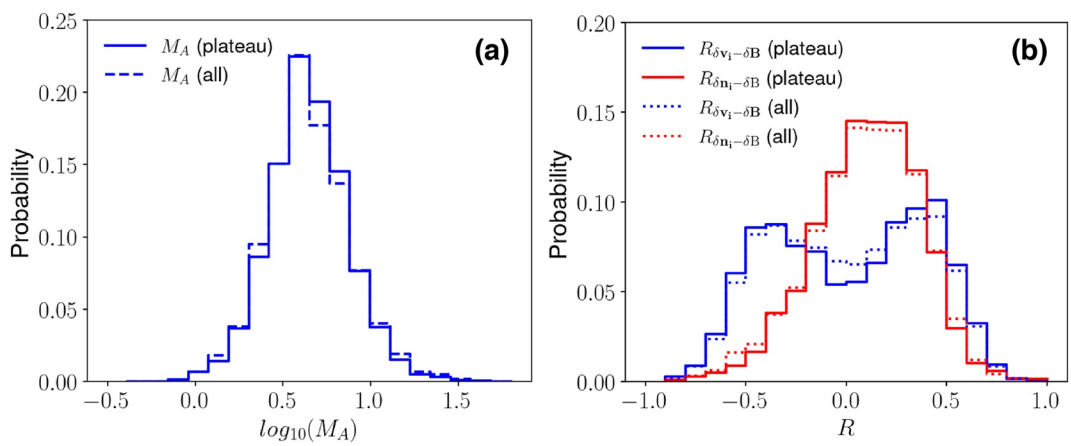

Figure 8. (a) Probability histograms of Alfvén Mach number considering plateau-like events only (solid) and all events (dashed). (b) Probability histograms of correlation coefficients between band-pass magnetic-field fluctuations, ion velocity fluctuations $R_{\delta \mathbf{v}_i - \delta B}$ (solid), and density fluctuations $R_{\delta \mathbf{n}_i - \delta B}$ (dotted) with frequency <0.015 Hz.

Data Availability Statement

The MAVEN spacecraft data used in this study are publicly available through the Planetary Data System: https://pds-ppi.igpp.ucla.edu/mission/MAVEN/MAVEN/MAG for MAG, https://pds-ppi.igpp.ucla.edu/mission/MAVEN/MAVEN/SWIA for SWIA and https://pds-ppi.igpp.ucla.edu/mission/MAVEN/MAVEN/STATIC for STATIC.

Acknowledgments
We thank the entire MAVEN team for providing the data. MAVEN data are publicly available through the Planetary Data System. We also thank Y. Harada for the helpful discussion. This work is supported by NNSFC Grants (42022032, 41874203, 42188101), project of Civil Aerospace "13th Five Year Plan" Preliminary Research in Space Science (D020301, D030202), Strategic Priority Research Program of CAS (Grant XDA17010301), and Key Research Program of Frontier Sciences CAS (Grant QYZDJ-SSW-JSC028). H. Li is also supported by International Partnership Program of CAS (Grant 183311KYSB20200017) and in part by the Specialized Research Fund for State Key Laboratories of China. D. V. is supported by the STFC Ernest Rutherford Fellowship ST/P003826/1 and STFC Consolidated Grants ST/S000240/1 and ST/W001004/1.

References

Alexandrova, O. (2008). Solar wind vs magnetosheath turbulence and Alfvén vortices. *Nonlinear Processes in Geophysics*, *15*(1), 95–108. https://doi.org/10.5194/npg-15-95-2008

Anderson, B. J., & Fuselier, S. A. (1993). Magnetic pulsations from 0.1 to 4.0 Hz and associated plasma properties in the Earth's subsolar magnetosheath and plasma depletion layer. *Journal of Geophysical Research*, *98*(A2), 1461–1479. https://doi.org/10.1029/92JA02197

Anderson, B. J., Fuselier, S. A., Gary, S. P., & Denton, R. E. (1994). Magnetic spectral signatures in the Earth's magnetosheath and plasma depletion layer. *Journal of Geophysical Research*, *99*(A4), 5877. https://doi.org/10.1029/93JA02827

Andrés, N., Romanelli, N., Hadid, L. Z., Sahraoui, F., DiBraccio, G., & Halekas, J. (2020). Solar wind turbulence around Mars: Relation between the energy cascade rate and the proton cyclotron waves activity. *The Astrophysical Journal*, *902*(2), 134. https://doi.org/10.3847/1538-4357/abb5a7

Barabash, S., Dubinin, E., Pissarenko, N., Lundin, R., & Russell, C. T. (1991). Picked-up protons near Mars: Phobos observations. *Geophysical Research Letters*, *18*(10), 1805–1808. https://doi.org/10.1029/91GL02082

Brain, D. A. (2002). Observations of low-frequency electromagnetic plasma waves upstream from the Martian shock. *Journal of Geophysical Research*, *107*(A6), 1076. https://doi.org/10.1029/2000JA000416

Bruno, R., & Carbone, V. (2013). The solar wind as a turbulence laboratory. *Living Reviews in Solar Physics*, *10*. https://doi.org/10.12942/lrsp-2013-2

Chamberlain, J. W. (1963). Planetary coronae and atmospheric evaporation. *Planetary and Space Science*, *11*(8), 901–960. https://doi.org/10.1016/0032-0633(63)90122-3

Chaufray, J.-Y., Gonzalez-Galindo, F., Forget, F., Lopez-Valverde, M., Leblanc, F., Modolo, R., & Hess, S. (2015). Variability of the hydrogen in the martian upper atmosphere as simulated by a 3D atmosphere–exosphere coupling. *Icarus*, *245*, 282–294. https://doi.org/10.1016/j.icarus.2014.08.038

Connerney, J. E. P., Espley, J., Lawton, P., Murphy, S., Odom, J., Oliversen, R., & Sheppard, D. (2015). The MAVEN magnetic field investigation. *Space Science Reviews*, *195*(1–4), 257–291. https://doi.org/10.1007/s11214-015-0169-4

Cowee, M. M., & Gary, S. P. (2012). Electromagnetic ion cyclotron wave generation by planetary pickup ions: One-dimensional hybrid simulations at sub-Alfvénic pickup velocities: Pickup ion waves in sub-alfvénic regime. *Journal of Geophysical Research*, *117*(A6), A06215. https://doi.org/10.1029/2012JA017568

Cowee, M. M., Russell, C. T., & Strangeway, R. J. (2008). One-dimensional hybrid simulations of planetary ion pickup: Effects of variable plasma and pickup conditions: Simulations of ion pickup conditions. *Journal of Geophysical Research*, *113*(A8). https://doi.org/10.1029/2008JA013066

Cravens, T. E., Hoppe, A., Ledvina, S. A., & McKenna-Lawlor, S. (2002). Pickup ions near Mars associated with escaping oxygen atoms: Pickup ions near Mars. *Journal of Geophysical Research*, *107*(A8), SMP 7-1–SMP 7-10. https://doi.org/10.1029/2001JA000125

Cravens, T. E., Kozyra, J. U., Nagy, A. F., Gombosi, T. I., & Kurtz, M. (1987). Electron impact ionization in the vicinity of comets. *Journal of Geophysical Research*, *92*(A7), 7341. https://doi.org/10.1029/JA092iA07p07341

Czaykowska, A., Bauer, T. M., Treumann, R. A., & Baumjohann, W. (2001). Magnetic field fluctuations across the Earth's bow shock. *Annales Geophysicae*, *19*(3), 275–287. https://doi.org/10.5194/angeo-19-275-2001

Delva, M., Bertucci, C., Volwerk, M., Lundin, R., Mazelle, C., & Romanelli, N. (2015). Upstream proton cyclotron waves at Venus near solar maximum. *Journal of Geophysical Research: Space Physics*, *120*(1), 344–354. https://doi.org/10.1002/2014JA020318

Dubinin, E., Fraenz, M., Woch, J., Barabash, S., Lundin, R., & Yamauchi, M. (2006). Hydrogen exosphere at Mars: Pickup protons and their acceleration at the bow shock. *Geophysical Research Letters*, *33*(22), L22103. https://doi.org/10.1029/2006GL027799

Dwivedi, N. K., Schmid, D., Narita, Y., Kovács, P., Vörös, Z., Delva, M., & Zhang, T. (2015). Statistical investigation on the power-law behavior of magnetic fluctuations in the Venusian magnetosheath. *Earth Planets and Space*, *67*(1), 137. https://doi.org/10.1186/s40623-015-0308-x

Eparvier, F. G., Chamberlin, P. C., Woods, T. N., & Thiemann, E. M. B. (2015). The solar extreme ultraviolet monitor for MAVEN. *Space Science Reviews*, *195*(1–4), 293–301. https://doi.org/10.1007/s11214-015-0195-2

Fite, W. L., Stebbings, R. F., Hummer, D. G., & Brackmann, R. T. (1960). Ionization and charge transfer in proton-hydrogen atom collisions. *Physical Review*, *119*(2), 663–668. https://doi.org/10.1103/PhysRev.119.663

Gary, S. P. (1991). Electromagnetic ion/ion instabilities and their consequences in space plasmas: A review. *Space Science Reviews*, *56*(3–4), 373–415. https://doi.org/10.1007/BF00196632

Gary, S. P., Fuselier, S. A., & Anderson, B. J. (1993). Ion anisotropy instabilities in the magnetosheath. *Journal of Geophysical Research*, *98*(A2), 1481–1488. https://doi.org/10.1029/92JA01844

Gary, S. P., & Madland, C. D. (1988). Electromagnetic ion instabilities in a cometary environment. *Journal of Geophysical Research*, *93*(A1), 235. https://doi.org/10.1029/JA093iA01p00235

Gary, S. P., & Winske, D. (1993). Simulations of ion cyclotron anisotropy instabilities in the terrestrial magnetosheath. *Journal of Geophysical Research*, *98*(A6), 9171. https://doi.org/10.1029/93JA00272

Hadid, L. Z., Sahraoui, F., Kiyani, K. H., Retinò, A., Modolo, R., Canu, P., et al. (2015). Nature of the MHD and kinetic scale turbulence in the magnetosheath of Saturn: *Cassini* observations. *The Astrophysical Journal*, *813*(2), L29. https://doi.org/10.1088/2041-8205/813/2/L29

Halekas, J. S., Ruhunusiri, S., Harada, Y., Collinson, G., Mitchell, D. L., Mazelle, C., et al. (2017). Structure, dynamics, and seasonal variability of the Mars-solar wind interaction: MAVEN solar wind ion analyzer in-flight performance and science results. *Journal of Geophysical Research: Space Physics*, *122*(1), 547–578. https://doi.org/10.1002/2016JA023167

Halekas, J. S., Taylor, E. R., Dalton, G., Johnson, G., Curtis, D. W., McFadden, J. P., et al. (2015). The solar wind ion analyzer for MAVEN. *Space Science Reviews*, *195*(1–4), 125–151. https://doi.org/10.1007/s11214-013-0029-z

Harada, Y., Ruhunusiri, S., Halekas, J. S., Espley, J., DiBraccio, G. A., Mcfadden, J. P., et al. (2019). Locally generated ULF waves in the martian magnetosphere: MAVEN observations. *Journal of Geophysical Research: Space Physics*, *124*(11), 8707–8726. https://doi.org/10.1029/2019JA027312

Huang, S. Y., Hadid, L. Z., Sahraoui, F., Yuan, Z. G., & Deng, X. H. (2017). On the existence of the Kolmogorov inertial range in the terrestrial magnetosheath turbulence. *The Astrophysical Journal*, *836*(1), L10. https://doi.org/10.3847/2041-8213/836/1/L10

Huang, S. Y., Wang, Q. Y., Sahraoui, F., Yuan, Z. G., Liu, Y. J., Deng, X. H., et al. (2020). Analysis of turbulence properties in the Mercury plasma environment using *MESSENGER* observations. *The Astrophysical Journal*, *891*(2), 159. https://doi.org/10.3847/1538-4357/ab7349

Huddleston, D. E., Strangeway, R. J., Blanco-Cano, X., Russell, C. T., Kivelson, M. G., & Khurana, K. K. (1999). Mirror-mode structures at the Galileo-Io flyby: Instability criterion and dispersion analysis. *Journal of Geophysical Research*, *104*(A8), 17479–17489. https://doi.org/10.1029/1999JA900195

Huddleston, D. E., Strangeway, R. J., Warnecke, J., Russell, C. T., Kivelson, M. G., & Bagenal, F. (1997). Ion cyclotron waves in the Io torus during the Galileo encounter: Warm plasma dispersion analysis. *Geophysical Research Letters*, *24*(17), 2143–2146. https://doi.org/10.1029/97GL01203

Jakosky, B. M., Lin, R. P., Grebowsky, J. M., Luhmann, J. G., Mitchell, D. F., Beutelschies, G., et al. (2015). The Mars Atmosphere and Volatile Evolution (MAVEN) mission. *Space Science Reviews*, *195*(1–4), 3–48. https://doi.org/10.1007/s11214-015-0139-x

Jian, L. K., Russell, C. T., Luhmann, J. G., Anderson, B. J., Boardsen, S. A., Strangeway, R. J., et al. (2010). Observations of ion cyclotron waves in the solar wind near 0.3 AU: Observations of ICWs near 0.3 AU. *Journal of Geophysical Research*, *115*(A12), A12115. https://doi.org/10.1029/2010JA015737

Klein, K. G., Howes, G. G., & TenBarge, J. M. (2014). The violation of the taylor hypothesis in measurements of solar wind turbulence. *The Astrophysical Journal*, *790*(2), L20. https://doi.org/10.1088/2041-8205/790/2/L20

Lentz, C. L., Chasapis, A., Qudsi, R. A., Halekas, J., Maruca, B. A., Andersson, L., & Baker, D. N. (2021). On the solar wind proton temperature anisotropy at Mars' orbital location. *Journal of Geophysical Research: Space Physics*, *126*(10), e2021JA029438. https://doi.org/10.1029/2021JA029438

Li, H., Jiang, W. C., Wang, C., Verscharen, D., Zeng, C., Russell, C. T., et al. (2020). Evolution of the Earth's magnetosheath turbulence: A statistical study based on MMS observations. *The Astrophysical Journal*, *898*(2), L43. https://doi.org/10.3847/2041-8213/aba531

Li, H., Li, N. W., Wang, C., & Yao, S. (2020). Plasma-beta modulated characteristics of magnetohydrodynamic waves around the heliospheric current sheet. *The Astrophysical Journal*, *889*(1), L16. https://doi.org/10.3847/2041-8213/ab698f

Maruca, B. A., Chasapis, A., Gary, S. P., Bandyopadhyay, R., Chhiber, R., Parashar, T. N., et al. (2018). MMS observations of beta-dependent constraints on ion temperature anisotropy in Earth's magnetosheath. *The Astrophysical Journal*, *866*(1), 25. https://doi.org/10.3847/1538-4357/aaddfb

Matsunaga, K., Seki, K., Brain, D. A., Hara, T., Masunaga, K., Mcfadden, J. P., et al. (2017). Statistical study of relations between the induced magnetosphere, ion composition, and pressure balance boundaries around Mars based on MAVEN observations: The MARTIAN plasma boundaries. *Journal of Geophysical Research: Space Physics*, *122*(9), 9723–9737. https://doi.org/10.1002/2017JA024217

Matteini, L., Schwartz, S., & Hellinger, P. (2015). Cometary ion instabilities in the solar wind. *Planetary and Space Science*, *119*, 3–12. https://doi.org/10.1016/j.pss.2015.08.016

McFadden, J. P., Kortmann, O., Curtis, D., Dalton, G., Johnson, G., Abiad, R., et al. (2015). MAVEN SupraThermal and thermal ion compostion (STATIC) instrument. *Space Science Reviews*, *195*(1–4), 199–256. https://doi.org/10.1007/s11214-015-0175-6

Modolo, R., Chanteur, G. M., Dubinin, E., & Matthews, A. P. (2005). Influence of the solar EUV flux on the Martian plasma environment. *Annales Geophysicae*, *23*(2), 433–444. https://doi.org/10.5194/angeo-23-433-2005

Pouquet, A., Frisch, U., & Léorat, J. (1976). Strong MHD helical turbulence and the nonlinear dynamo effect. *Journal of Fluid Mechanics*, *77*(2), 321–354. https://doi.org/10.1017/S0022112076002140

Pouquet, A., Stawarz, J. E., & Rosenberg, D. (2020). Coupling large eddies and waves in turbulence: Case study of magnetic helicity at the ion inertial scale. *Atmosphere*, *11*(2), 203. https://doi.org/10.3390/atmos11020203

Rahmati, A., Cravens, T. E., Nagy, A. F., Fox, J. L., Bougher, S. W., Lillis, R. J., et al. (2014). Pickup ion measurements by MAVEN: A diagnostic of photochemical oxygen escape from Mars: Photochemical oxygen escape from Mars. *Geophysical Research Letters*, *41*(14), 4812–4818. https://doi.org/10.1002/2014GL060289

Rahmati, A., Larson, D. E., Cravens, T. E., Lillis, R. J., Halekas, J. S., McFadden, J. P., et al. (2017). MAVEN measured oxygen and hydrogen pickup ions: Probing the Martian exosphere and neutral escape. *Journal of Geophysical Research: Space Physics*, *122*(3), 3689–3706. https://doi.org/10.1002/2016JA023371

Rahmati, A., Larson, D. E., Cravens, T. E., Lillis, R. J., Halekas, J. S., McFadden, J. P., et al. (2018). Seasonal variability of neutral escape from Mars as derived from MAVEN pickup ion observations. *Journal of Geophysical Research: Planets*, *123*(5), 1192–1202. https://doi.org/10.1029/2018JE005560

Rakhmanova, L., Riazantseva, M., Zastenker, G., & Verigin, M. (2018). Kinetic-scale ion flux fluctuations behind the quasi-parallel and quasi-perpendicular bow shock. *Journal of Geophysical Research: Space Physics*, *123*(7), 5300–5314. https://doi.org/10.1029/2018JA025179

Rakhmanova, L., Riazantseva, M., Zastenker, G., Yermolaev, Y., & Lodkina, I. (2020). Dynamics of plasma turbulence at Earth's bow shock and through the magnetosheath. *The Astrophysical Journal*, *901*(1), 30. https://doi.org/10.3847/1538-4357/abae00

Remya, B., Reddy, R. V., Tsurutani, B. T., Lakhina, G. S., & Echer, E. (2013). Ion temperature anisotropy instabilities in planetary magnetosheaths: ION instabilities in the magnetosheath. *Journal of Geophysical Research: Space Physics*, *118*(2), 785–793. https://doi.org/10.1002/jgra.50091

Riazantseva, M., Budaev, V., Rakhmanova, L., Zastenker, G., Šafránková, J., Němeček, Z., & Přech, L. (2016). Comparison of properties of small-scale ion flux fluctuations in the flank magnetosheath and in the solar wind. *Advances in Space Research*, *58*(2), 166–174. https://doi.org/10.1016/j.asr.2015.12.022

Romanelli, N., Andrés, N., & DiBraccio, G. A. (2022). Variability of the incompressible energy cascade rate in solar wind turbulence around Mars. *The Astrophysical Journal*, *929*(2), 145. https://doi.org/10.3847/1538-4357/ac5902

Romanelli, N., Bertucci, C., Gómez, D., Mazelle, C., & Delva, M. (2013). Proton cyclotron waves upstream from Mars: Observations from Mars global surveyor. *Planetary and Space Science*, *76*, 1–9. https://doi.org/10.1016/j.pss.2012.10.011

Romanelli, N., Mazelle, C., Chaufray, J. Y., Meziane, K., Shan, L., Ruhunusiri, S., et al. (2016). Proton cyclotron waves occurrence rate upstream from Mars observed by MAVEN: Associated variability of the martian upper atmosphere: Temporal variability of PCWs. *Journal of Geophysical Research: Space Physics*, *121*(11), 11113–11128. https://doi.org/10.1002/2016JA023270

Ruhunusiri, S., Halekas, J. S., Espley, J. R., Mazelle, C., Brain, D., Harada, Y., et al. (2017). Characterization of turbulence in the Mars plasma environment with MAVEN observations. *Journal of Geophysical Research: Space Physics*, *122*(1), 656–674. https://doi.org/10.1002/2016JA023456

Russell, C. T., Huddleston, D. E., Strangeway, R. J., Blanco-Cano, X., Kivelson, M. G., Khurana, K. K., et al. (1999). Mirror-mode structures at the Galileo-IO flyby: Observations. *Journal of Geophysical Research*, *104*(A8), 17471–17477. https://doi.org/10.1029/1999JA900202

Sahraoui, F., Hadid, L., & Huang, S. Y. (2020). Magnetohydrodynamic and kinetic scale turbulence in the near-Earth space plasmas: A (short) biased review. *Reviews of Modern Plasma Physics*, *4*(1), 4. https://doi.org/10.1007/s41614-020-0040-2

Song, P., Russell, C. T., & Thomsen, M. F. (1992). Waves in the inner magnetosheath: A case study. *Geophysical Research Letters*, *19*(22), 2191–2194. https://doi.org/10.1029/92GL02499

Taylor, G. I. (1937). The spectrum of turbulence. *Proceedings of Royal Society of London Series* A, *164*(919), 476–490. https://doi.org/10.1098/rspa.1938.0032

Terres, M., & Li, G. (2021). Relating the solar wind turbulence spectral break at the dissipation range with an upstream spectral bump at planetary bow shocks. arXiv:2108.07048 [physics].

Tu, C. Y., & Marsch, E. (1995). MHD structures, waves and turbulence in the solar wind: Observations and theories. *Space Science Reviews*, *73*(1–2), 1–210. https://doi.org/10.1007/BF00748891

Verscharen, D., Klein, K. G., & Maruca, B. A. (2019). The multi-scale nature of the solar wind. *Living Reviews in Solar Physics*, *16*(1), 5. https://doi.org/10.1007/s41116-019-0021-0

Vörös, Z., Zhang, T. L., Leubner, M. P., Volwerk, M., Delva, M., & Baumjohann, W. (2008). Intermittent turbulence, noisy fluctuations, and wavy structures in the Venusian magnetosheath and wake. *Journal of Geophysical Research*, *113*, E00B21. https://doi.org/10.1029/2008JE003159

Vörös, Z., Zhang, T. L., Leubner, M. P., Volwerk, M., Delva, M., Baumjohann, W., & Kudela, K. (2008). Magnetic fluctuations and turbulence in the Venus magnetosheath and wake. *Geophysical Research Letters*, *35*(11), L11102. https://doi.org/10.1029/2008GL033879